Open Access

Catalysis Research

LIDSEN Publishing Inc.

Original Research

Homogeneous {Ti_2Ni} Heterotrinuclear Catalyst for Ethylene Polymerization and Copolymerization

Luiz Felipe da M. Rocha [1], Leonardo C. Ferreira [1,*], Maria de Fátima V. Marques [1,*], Rodrigo S. Bitzer [2], Marco Antonio Chaer Nascimento [2]

1. Instituto de Macromoléculas Professora Eloisa Mano, Universidade Federal do Rio de Janeiro, Cidade Universitária – Centro de Tecnologia – Bloco J. POBox 68525. Rio de Janeiro – RJ, 21945-970, Brazil; E-Mails: luilipe@hotmail.com; mravel4@yahoo.com.br; fmarques@ima.ufrj.br
2. Instituto de Química, Universidade Federal do Rio de Janeiro, Cidade Universitária – Centro de Tecnologia – Bloco A. Rio de Janeiro – RJ, 21941-909, Brazil; E-Mails: rbitzer@gmail.com; mnascimento@gmail.com

* **Correspondences:** Leonardo C. Ferreira and Maria de Fátima V. Marques; E-Mails: mravel4@yahoo.com.br; fmarques@ima.ufrj.br

Academic Editors: Luísa Margarida Martins and Amoolya Dattatraya Lalsare

Special Issue: Hetero-/Homo-geneous Catalysis in Organic Synthesis and Sustainable Chemistry

Catalysis Research
2022, volume 2, issue 3
doi:10.21926/cr.2203020

Received: May 18, 2022
Accepted: June 26, 2022
Published: July 06, 2022

Abstract

We synthesized and spectroscopically characterized a new heterotrimetallic {Ti_2Ni} ethylene (co)polymerization precatalyst containing one (α-diimine)$NiBr_2$ and two (phenoxy-imine)$TiCl_4$ scaffolds. Its calculated structure was investigated at the DFT B3LYP/LACVP** level. Our calculations showed that the titanium(IV) centers were in a slightly distorted trigonal bipyramidal environment, and the average Ti···Ni distance was 8.76 Å. The precatalyst was used for synthesizing polyethylene and ethylene copolymers. The results of GPC analyses showed that the obtained polyethylenes had the desired bimodal molecular weight distributions. The FTIR spectra revealed that polydispersity decreased as the vinyl end-group content increased. These results suggested that high mechanical resistance can increase the mechanical energy needed for processing the material. All ^{13}C NMR signals were assigned to

short-chain branches with specific spatial arrangements along the polymer backbone. The chain walking mechanism of branch formation controls the spacing and conformational arrangements between these short chains.

Keywords
Heterotrinuclear catalyst; polymerization; polyethylene; homogeneous catalysis

1. Introduction

Two or more metal centers synergically act in the active site of several enzymes, thus improving kinetics and imparting high selectivity [1, 2]. Based on this mechanism of action, multinuclear cooperative catalysis has been applied to many processes, including coordination polymerization, olefin hydrogenation, hydroformylation, cycloaddition, and epoxidation [3-5]. In olefin polymerization reactions catalyzed by multinuclear transition metal complexes, cooperative effects significantly enhance the molecular weight, chain branch density, and comonomer enchainment selectivity of the products compared to the reactions catalyzed by analogous mononuclear catalysts [6, 7]. Thus, using heterotrinuclear catalysts allow several tandem reactions to be studied. Different metal backbones facilitate mechanistically different cycles and can cooperatively operate during the catalytic cycle [8].

Both homo and heterodinuclear complexes containing metals of groups 4 and 6 (e.g., Ti_2, Zr_2, Ti−Zr, and Ti−Cr) exhibit distinctive cooperative effects in the production of polyolefins with substantially higher molecular weights (M_w's) and comonomer enchainment contents, compared to the corresponding mononuclear analogs [9-13].

Since the 1950s, Ziegler-Natta catalysis has evolved from developing several homogeneous metallocenes based on early transition metals [14, 15]. In the 1990s, Brookhart et al. polymerized α-olefins catalyzed by nickel(II) and palladium(II) α-diimine complexes that were activated by methylaluminoxane (MAO) or other ionizing agents [16]. Polyethylenes synthesized using Brookhart catalysts have highly linear to moderately branched structures. Methyl branches predominate due to variations in the catalyst structure, comonomer, temperature, and ethylene pressure [17, 18].

In the same decade, group 4 metal phenoxy-imine catalysts developed by scientists at Mitsui & Co. suggested an attractive class of living olefin polymerization [19]. Fujita et al. reported several non-metallocene catalytic systems for ethylene polymerization, consisting of titanium complexes bearing two chelating phenoxy-imine ligands and MAO (Ti-FI catalysts) [20, 21].

Mixtures of titanium and nickel complexes are used to produce a wide range of branched polyethylenes [22, 23]. However, studies on polymerization catalysts based on heterometallic complexes containing metals of groups 4 and 10 are limited [24]. In this study, we reported the catalytic activity for the ethylene (co)polymerization of a new trimetallic {Ti_2Ni} complex. This complex had two titanium(IV) centers bound to chelating phenoxy-imine groups connected by a central (°iamine)nickel(II) scaffold. We hypothesized that cooperative effects involving two or more metal centers might lead to more efficient chain propagation and/or new polymer architectures.

2. Materials and Methods

2.1 Synthesis of the N1C1 Complex

The reaction scheme is shown in Figure 1. Sufficient quantities of the **N1C1** complex were synthesized using the one-pot reaction technique [25].

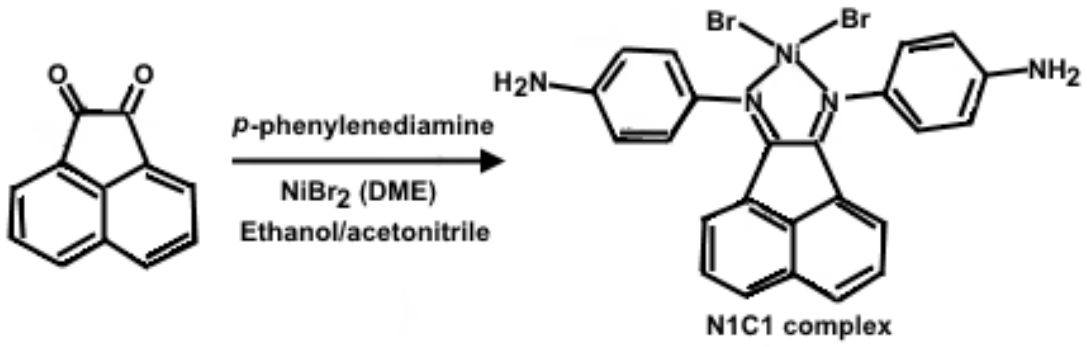

Figure 1 Synthesis of the **N1C1** complex.

In a 100 mL Schlenk flask, 0.466 g (2.0 mmol) of acenaphthenequinone, 0.540 g (5.0 mmol) of *p*-phenylenediamine, 0.718 g (1.7 mmol) of $NiBr_2$(DME) (DME = ethylene glycol dimethyl ether), 10 mL of acetonitrile, and 40 mL of ethanol were added. The reaction was performed under reflux for 3 h at 80°C. Subsequently, the product was filtered, washed three times with 10 mL of hexane, and dried under vacuum. The yield was 84%. Elemental Analysis CHN: % C Calc. (50.13) Found: (50.70); % H Calc. (2.08) Found (2.14); % N Calc. (9.75) Calc. (9.88). FTIR (KBr, 4,000–600 cm^{-1}): vC=N 1,586 cm^{-1}, and vN-H 3,500 cm^{-1}.

2.2 Synthesis of the N1C2 Complex

The reaction scheme is shown in Figure 2. In a 100 mL Schlenk flask, 0.274 g (1.2 mmol) of 3,5-di-*tert*-butylsalicylaldehyde, 0.350 g (0.60 mmol) of **N1C1**, 10 mL of acetonitrile, 10 mL of dichloromethane, and 30 mL of ethanol were added. The reaction was refluxed for 3 h at 80°C. Then, the product was filtered, washed three times with 10 mL of hexane, and dried under vacuum. The yield was 49%. Elemental Analysis CHN: % C Calc. (64.41) Found: (64.94); % H Calc. (5.17) Found (5.56); % N Calc. (5.56) Found: (5.80). UV-Vis (λmax, nm) in $CHCl_3$: 271, 328, and 381. FTIR (Nujol, 4,000–200 cm^{-1}): vC=N 1,611 cm^{-1}, vO-H 3,600 cm^{-1}, vC-H 2,920 cm^{-1}, vNi-N 535 cm^{-1}, and vNi-Br 235 cm^{-1}.

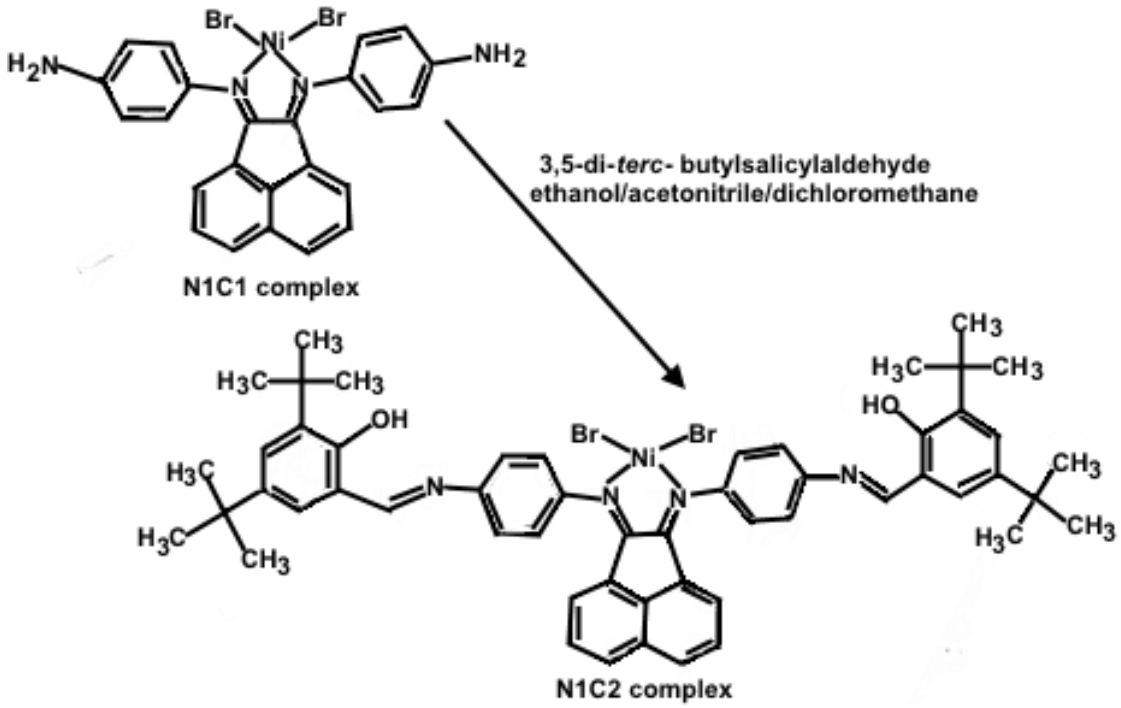

Figure 2 Synthesis of the **N1C2** complex.

2.3 Synthesis of the C1 Complex

The reaction scheme is shown in Figure 3. In a 100 mL Schlenk flask containing 30 mL of THF, 0.114 g (0.12 mmol) of **N1C2** was added. This solution was homogenized at room temperature for 20 min. Then, it was transferred dropwise to another Schlenk flask containing a solution of 0.54 mL (0.24 mmol) of $TiCl_4$ in 30 mL of THF. After stirring for 2 h at room temperature, the solution was filtered, and the resulting solid was washed three times with 10 mL of hexane and dried under a vacuum. The yield was 20%. Elemental Analysis CHN: % C Calc. (49.35) Found (49.99); % H Calc. (3.81) Found (3.70); % N Calc. (4.26) Found (4.20). UV-Vis (λ_{max}, nm) in $CHCl_3$: 328 and 381. FTIR (Nujol, 4,000–200 cm^{-1}): vC=N 1,580 cm^{-1}, vC-H 2,885 cm^{-1}, vNi-N 535 cm^{-1}, vNi-Br 235 cm^{-1}, vTi-N 490 cm^{-1}, vTi-O 350 cm^{-1}, and vTi-Cl 310 cm^{-1}.

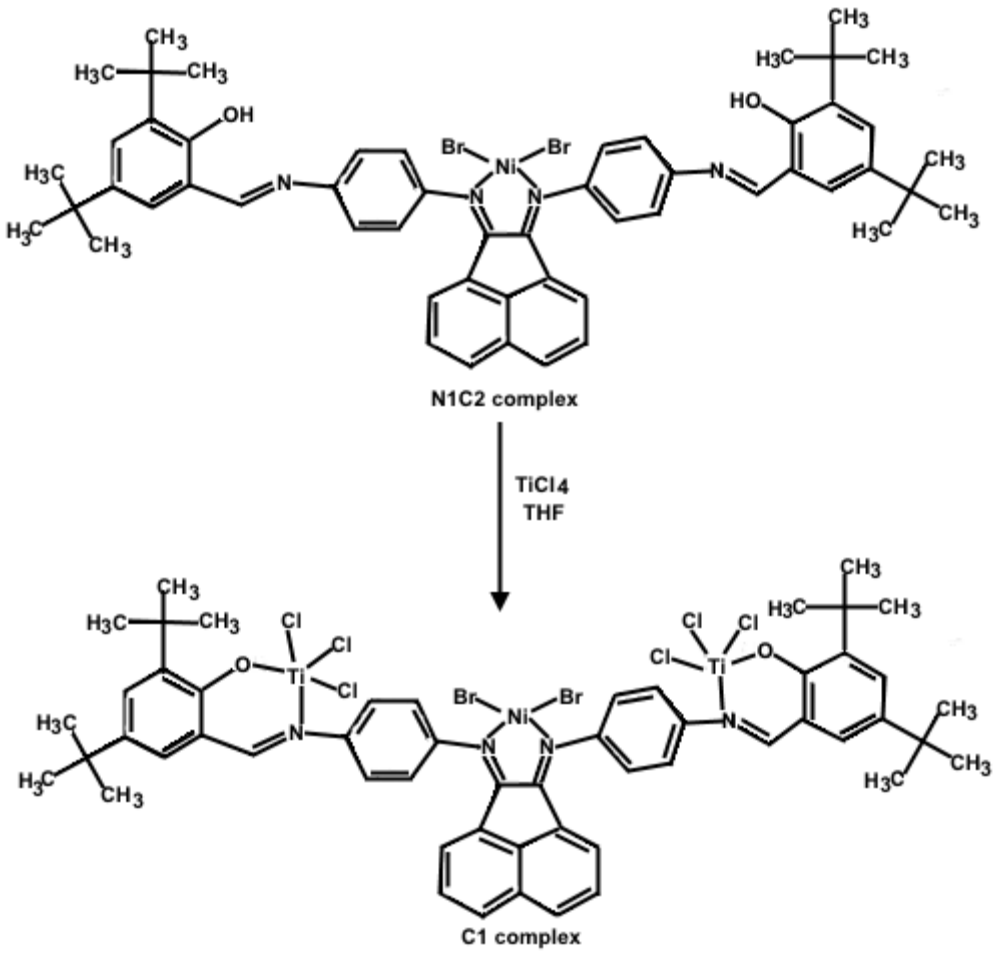

Figure 3 Synthesis of the **C1** complex.

2.4 Computational Details

All calculations were performed with JAGUAR 7.9 following an energy convergence criterion of 1.00×10^{-8} Hartree [26]. Gas-phase geometry optimizations were performed without constraints using the B3LYP hybrid functional and the LACVP** basis set [27]. We evaluated the vibrational frequencies of each optimized geometry at the same level of calculation and verified whether they were real. The experimental and calculated frequencies showed excellent agreement.

2.5 Ethylene Polymerization

Ethylene polymerization was performed in duplicate (error up to 13% in yield) in a Büchi 280 GlassUster BEP reactor using a 1,000 mL beaker coupled to a mechanical stirrer; the system was maintained at 650 rpm during polymerization. The pressure maintained was 0.4 MPa and the reactions were performed at 25, 50, and 70°C for 1 h.

2.6 Polymer Characterization

Differential scanning calorimetry (equipment Q1000, TA Instruments) was performed to determine the melting temperature™, the melting enthalpy (ΔH_m), and the crystallinity index (CI) of the polymers obtained. The samples were heated from 20 to 180°C and held at 180°C for 5 min to

eliminate the thermal history; then, the samples were cooled and heated at the same rate. In the second heating phase, the T_m and ΔH_m of the material were recorded. The crystallinity index (CI) was calculated using ΔH_m^{100} = 293 J/g.

The unsaturation of the polymer was analyzed using a PerkinElmer Spectrum Version 10.4.2 FTIR spectrometer with attenuated total reflectance (ATR) accessory using film samples. The concentrations of end-groups vinyl, trans-vinylene, and vinylidene were determined from the absorptions at 910 cm^{-1}, 965 cm^{-1}, and 888 cm^{-1}, respectively [28].

The ^{13}C NMR spectra (Figure 4) were obtained with a Bruker DPX-200 spectrometer, operating at 75 MHz. An 80 mg aliquot of each sample and 2 mL of o-trichloroethylene (TCE) were mixed in the NMR tubes (10 mm) and heated to 120°C for 8–12 h. The ^{13}C NMR spectra were also obtained at 120°C. In the polymer solutions, 1 mL of benzene-d6 was added to provide the internal lock signal. The chemical shifts were referenced internally to the major backbone methylene carbon resonance, taken as 30.00 ppm from Me4Si. Spectra were taken with a 90° flip angle, an acquisition time of 1.5 s, and a delay of 10 s.

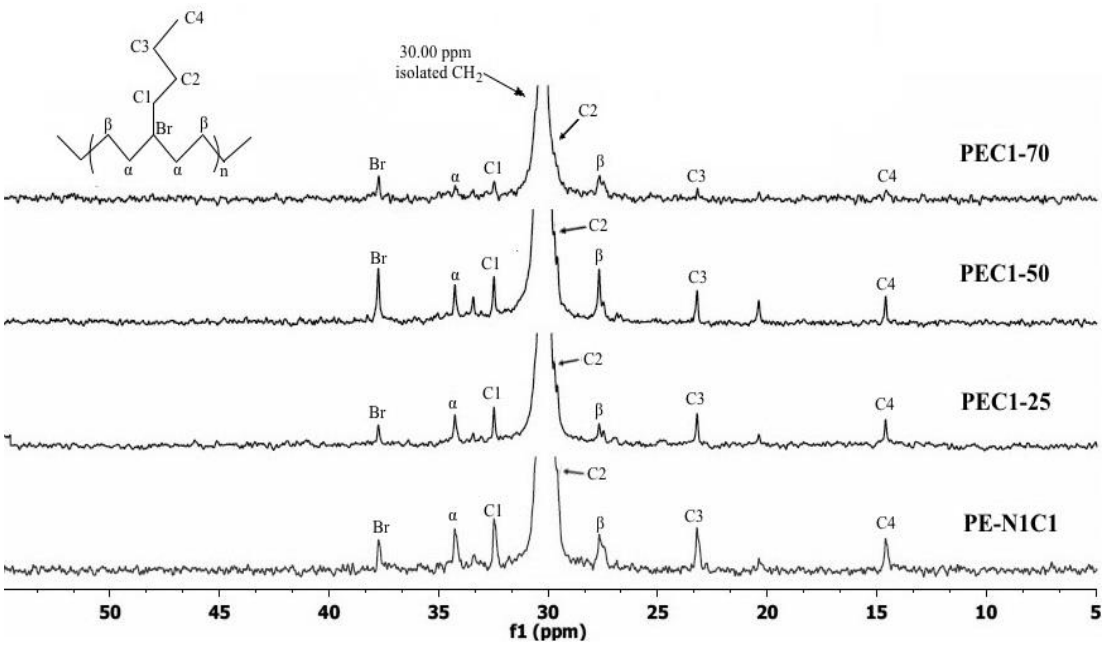

Figure 4 The ^{13}C NMR spectra (75 MHz, $C_2D_2Cl_4$, 120°C) of the PEs produced by the mononuclear {Ni} catalyst **N1C1**, and the heterotrinuclear {Ti···Ni} catalyst **C1** (Table 1), scaled to the PE CH_2 backbone resonance at 30.00 ppm.

Table 1 Data on ethylene polymerization for precatalysts **N1C1** and **C1**.

Sample	Temp (°C)	[a]PE (g)	[b]Activity (g.mmol^{-1})	[c]Amount of vinyl (in 1000 C)	Methyl branch (%) (in 1000 C)	Other branches (%) (in 1000 C)	[e]T_m (°C)	[e]ΔH (J/g)	*CI* (%)	*f*M_n (g.mol^{-1})	*f*M_w (g.mol^{-1})	[f]PDI
PE-N1C1	25	1.5	2000	0.6	22	77	125	190	65	3367	59.500	17.7
PEC1–25	25	0.9	740	0.6	25	60	127	206	70	2653	314.845	118.7
PEC1–50	50	0.6	557	0.5	36	63	128	177	60	3147	461.081	146.5
PEC1–70	70	0.6	483	1.1	53	45	129	127	43	6201	286.992	46.3

Conditions: 0.02 mmol of catalyst; Al/Metals = 250 to N1C1 and 125 to C1 (Al/Me = 125 to each metal center); ethylene pressure = 4 atm; toluene = 150 ml; each polymerization was performed in duplicate; [a]in units of (g of PE)·(mol of catalyst)$^{-1}$·h^{-1}·atm^{-1}; [b]in units of (kg of PE)·(mol of catalyst)$^{-1}$·h^{-1}·atm^{-1}; [c]determined by FTIR; [d]determined by ^{13}C NMR analysis.19; [e]melting temperature, enthalpy, and crystallinity index (CI) e as determined by differential scanning calorimetry; [f]GPC vs. polystyrene standards.

The molecular weight and molecular weight dispersity of the polymer samples were determined by performing Gel Permeation Chromatography (GPC) with a PL-GPC 220 High-Temperature Chromatograph (Agilent, UK) equipped with a differential refractive index (RI) detector. The samples (4 mg) were dissolved in 2 mL of 1,2,4-trichlorobenzene (TCB) for at least 3 h with 0.025% butylated hydroxytoluene (BHT), which acted as a stabilizer to prevent sample decomposition/degradation. TCB with 0.0125% BHT was used as the mobile phase at a flow rate of 1 mL min^{-1}. The 7.5 mm^2 PLgel Olexis columns (Agilent Technologies, UK) were combined with 7.5 mm^2 PLgel Olexis guard columns, into which each sample was injected. All HT-SEC experiments were performed at 150°C. The instrument was calibrated using narrowly distributed polystyrene standards (Agilent Technologies, UK).

3. Results and Discussion

3.1 Synthesis, Spectroscopy, and DFT Calculations

All complexes reported in this study were obtained as analytically pure solids, confirmed by performing elemental analyses and FTIR spectroscopy. The FTIR spectrum of **N1C1** showed a ν(C=N) + ν(C=C) band at 1,586 cm^{-1}, which was similar to that found in previous studies [29, 30]. Additionally, ν(N-H) bands were observed around 3,500 cm^{-1}, and bands assigned to aromatic C-H vibrations appeared around 3,030 cm^{-1}.

As expected, the ν(N-H) bands were not found in the FTIR spectrum of **N1C2**. Moreover, a strong ν(C=N) + ν(C=C) band was found at 1,611 cm^{-1} and a broad ν(O-H) band centered at 3,600 cm^{-1}. The low-frequency FTIR spectrum of **N1C2** showed two medium-intensity bands located at 535 and 235 cm^{-1}, attributed to ν(Ni-N) and ν(Ni-Br), respectively [31].

In the FTIR spectra of **C1**, the coupled ν(C=N) + ν(C=C) band was located at 1,580 cm^{-1}. This shift suggested the coordination of $TiCl_4$ to the free iminic groups in **C1**. The other change was the disappearance of vibrations relating to the phenolic O-H group, indicating the coordination of this group to the titanium(IV) centers. The low-frequency FTIR spectrum of **C1** exhibited the same absorptions attributed to ν(Ni-N) and ν(Ni-Br), i.e., 534 and 235 cm^{-1}, respectively, besides the vibrations located at 490, 310, and 350 cm^{-1}, attributed to ν(Ti-N), ν(Ti-O) and ν(Ti-Cl), respectively [31]. The main absorption bands and respective assignments of the three complexes are presented in Table 2.

Table 2 The FTIR bands (cm^{-1}) for **N1C1**, **N1C2**, and **C1**.

Complex	ν N-H (cm^{-1})	ν C=N diimine (cm^{-1})	ν C=N + ν C=C (cm^{-1})	ν C=N phenoxy-imine (cm^{-1})	ν O-H phenol (cm^{-1})	ν C-H aromatic (cm^{-1})	ν C-H alkyl (cm^{-1})
N1C1	3500 m	Coupled to C=C	1586 vs	-	-	3030 m	-
N1C2	-	Coupled to C=C	1586 vs	1611 vs	3600 s	3032 m	2720 w
C1	-	Coupled to C=C	1580 vs	Coupled to C=C	-	3035 m	2718 w

Weak (w); strong (s); very strong (vs); medium (m); stretching (ν).

The calculated structure of **N1C1**, **N1C2,** and **C1** were examined by density functional theory at the B3LYP/LACVP** level. The optimized structure for **N1C1** is shown in Figure 5. As expected, this complex could inhibit a square-planar nickel(II) center attached to two nitrogen atoms and two bromides. Besides, all bond lengths showed the expected values [32]. The structure showed a bite angle (N1-Ni-N2) of 82.3°, which was consistent with those found in other square-planar (α-diimines)nickel(II) complexes.

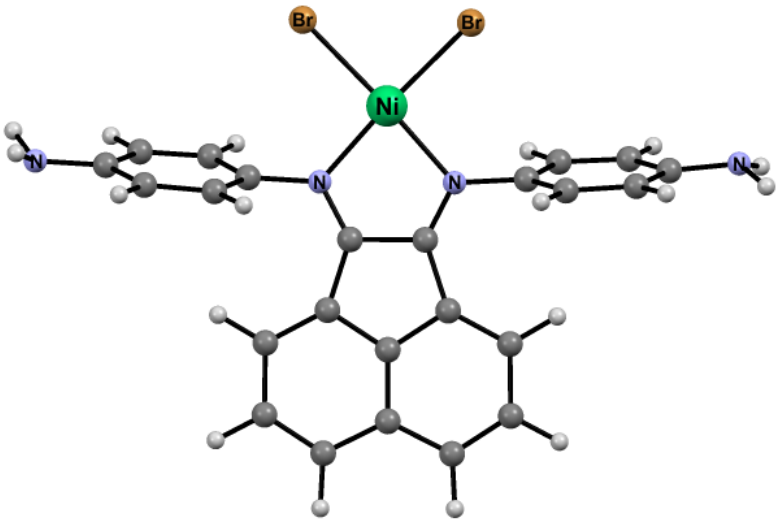

Figure 5 The structure of **N1C1** was optimized at the B3LYP/LACVP** calculation level.

The optimized structure for **N1C2** was similar to that found in the results of our experiment (Figure 6). As expected, the coordination geometry of **N1C2** was the same as that of its precursor, and their geometric parameters were very similar.

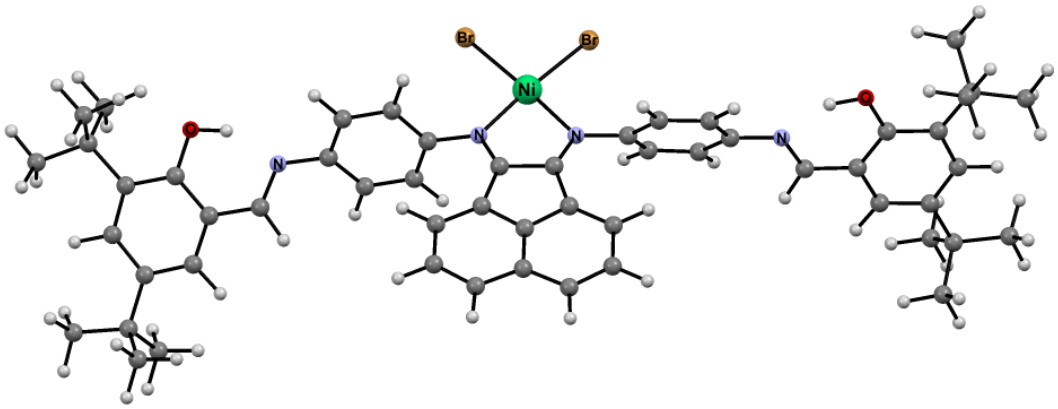

Figure 6 The structure of **N1C2** was optimized at the B3LYP/LACVP** calculation level.

Two different isomers, i.e., *syn* and *anti*, were optimized for **C1** (Figure 7). According to our calculations, *anti*-**C1** was 7.4 kcal mol^{-1} and was more stable than the *syn*-**C1**. The *anti*-**C1** conformer had five-coordinate titanium(IV) centers in a distorted trigonal bipyramidal coordination environment, with Addison's geometry indices (τ_5) [33] around 0.93. Moreover, all bond lengths were of the expected values [32]. Three polymerization centers were present in *anti*-**C1**. Its average Ti···Ni distance (8.76 Å) suggested that cooperativity/synergy between these reactive sites might be possible.

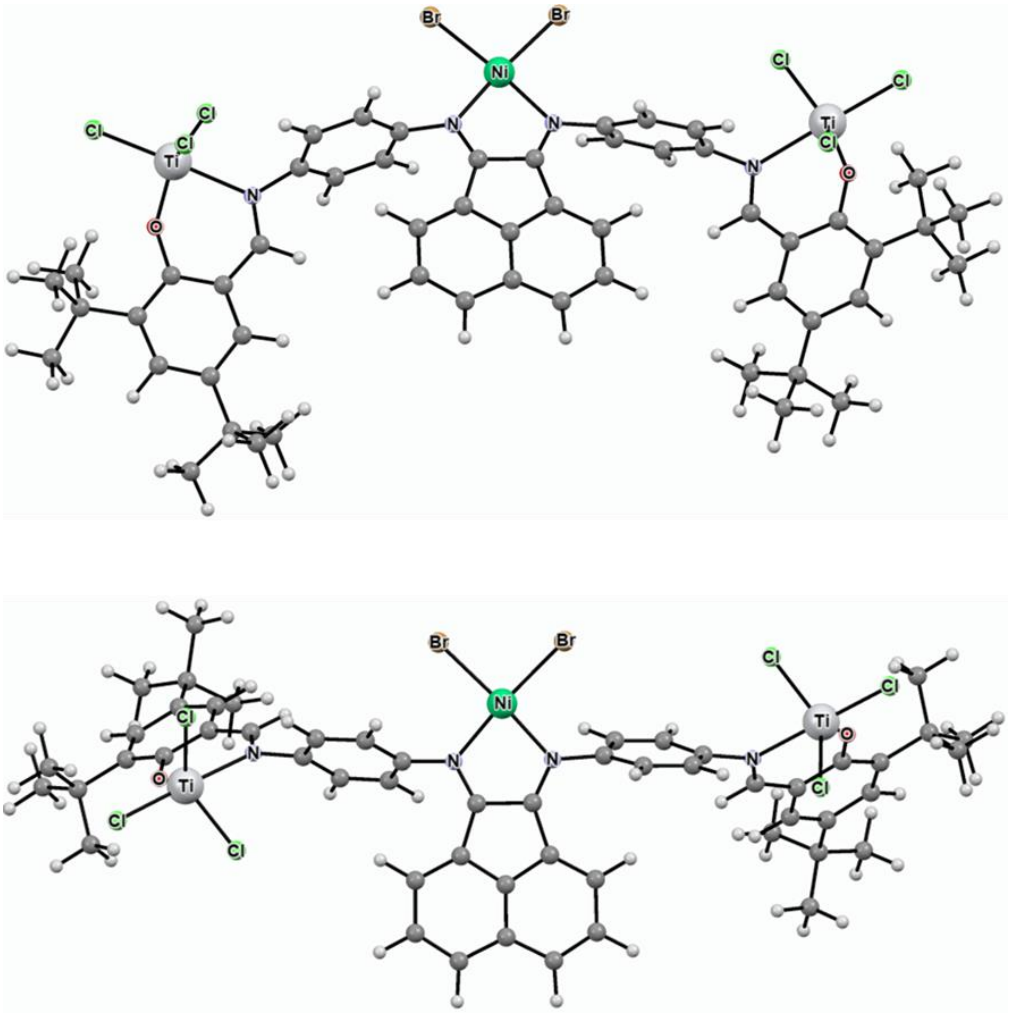

Figure 7 The structures for *syn*-**C1** (top) and *anti*-**C1** (bottom) were optimized at the B3LYP/LACVP** calculation level.

3.2 Polymerization Reactions

Ethylene polymerization reactions were conducted using **C1**/MAO as a catalytic system in toluene at a constant ethylene pressure (4 atm). Initially, we found that the **N1C1**/MAO system had the highest activity but produced polyethylene with a lower molecular weight and polydispersity index (PDI) (Table 1). The N1C1 catalyst contains NH_2 groups, which can be metalized by aluminum alkyls under the conditions used. The electronic effect of these-NH_2 or [Al](H)N-groups can be increased and can dramatically influence the performance of the respective catalyst. This explains the high PDI of this single-site catalyst (with PDI = 2), indicating that these groups increased the chain transfer reactions.

The polydispersity index increased sharply for polyethylenes synthesized with the trinuclear catalyst than that synthesized with the mononuclear catalyst, as expected. Also, the melting temperature was slightly higher. The fact that T_m was higher in the polymer produced with **C1** catalyst at 70°C while the degree of crystallinity was the lowest indicated that two different fractions of polyethylene were produced, one with few branches and the other with many branches.

Surprisingly, the C1 catalyst with two phenoxy-imine ligands polymerized ethylene with moderate activities. At the beginning of polymerization, rapid formation of the bulk polymer was

observed. The reaction might have been limited by monomer diffusion due to the presence of insoluble polymers, especially for PEC1–70 [34].

Similar activities at different temperatures using **C1** were considerably different from the activity using **N1C1**, which suggested a synergistic effect in the presence of three metal centers. In some cases, multinuclear catalysts exhibit lower activities than their mononuclear counterparts, probably reflecting steric and electronic constraints [35].

3.3 Gel Permeation Chromatography (GPC)

The polymers produced using the **N1C1** mononuclear precatalyst had lower molecular weights (M_w) than those synthesized using **C1**. This was probably because of the higher frequency of chain transfer reactions to-NH_2 groups and the lower steric hindrance of the aniline moiety in **N1C1**. Nickel(II) diimine complexes that lack bulky substituents generally favor chain transfer by β-H elimination (chain transfer process by chain walking mechanism) concerning chain propagation [36, 37].

The polymerization temperature influenced the activity, molecular weight, and polymer architecture when a heterotrinuclear catalyst was used. Polymerization reactions were performed at 25, 50, and 70°C.

While the activity decreased with an increase in the polymerization temperature, the molecular weight (M_w) was the highest at 50°C. For the three conditions, the concentration of polyethylene with vinyl-end groups increased with an increase in the reaction temperature due to an increase in the rate of the β-H elimination reactions [38]. The polydispersity increased significantly at 25 and 50°C, indicating that this polymer fraction increases within this temperature range.

The representative molecular weight distributions for the polymers that presented different molecular weights and polydispersities are shown in Figure 8. The molecular weight distribution was considerably wider for the polymers produced by the heterotrinuclear catalyst, which indicated the presence of polymer blends with different molecular weights.

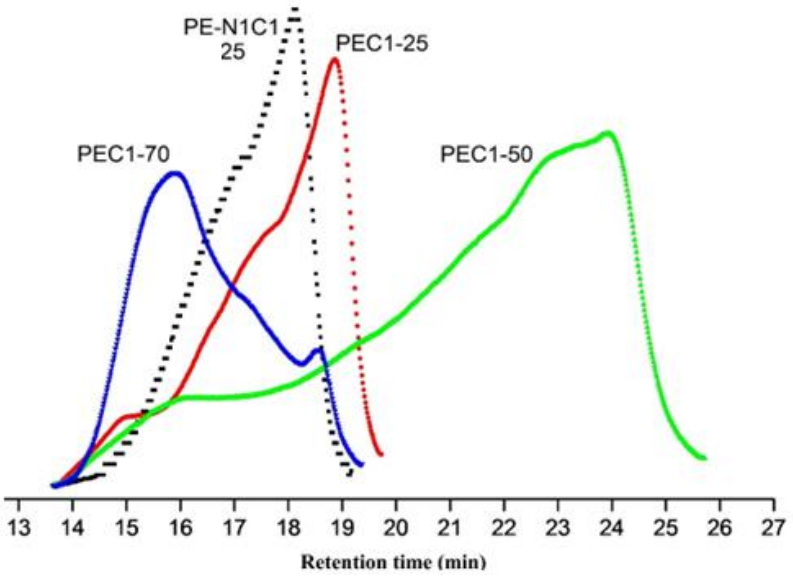

Figure 8 GPC of polyethylenes derived from **N1C1** (mononuclear catalyst) (black line) and **C1** (heteronuclear catalyst).

3.4 Unsaturation and Branching Contents

The vinyl index was the ratio between the integrated absorption band of the vinyl groups and that of the CH_2 group (1,470 cm^{-1}) [39]. The results of the FTIR analysis of the vinyl end-groups (Figure 9) showed that the unsaturation was consistent with β-H elimination and double bond migration [29]. Therefore, many short-chain branches were produced at Ni sites via β-H elimination. These chains were then efficiently reinserted intramolecularly through Ti sites, resulting in long chains of highly branched polymers. The cooperative effects involving the elimination of macromonomers and intramolecular reinsertion in different sites enabled heterotrinuclear catalysis.

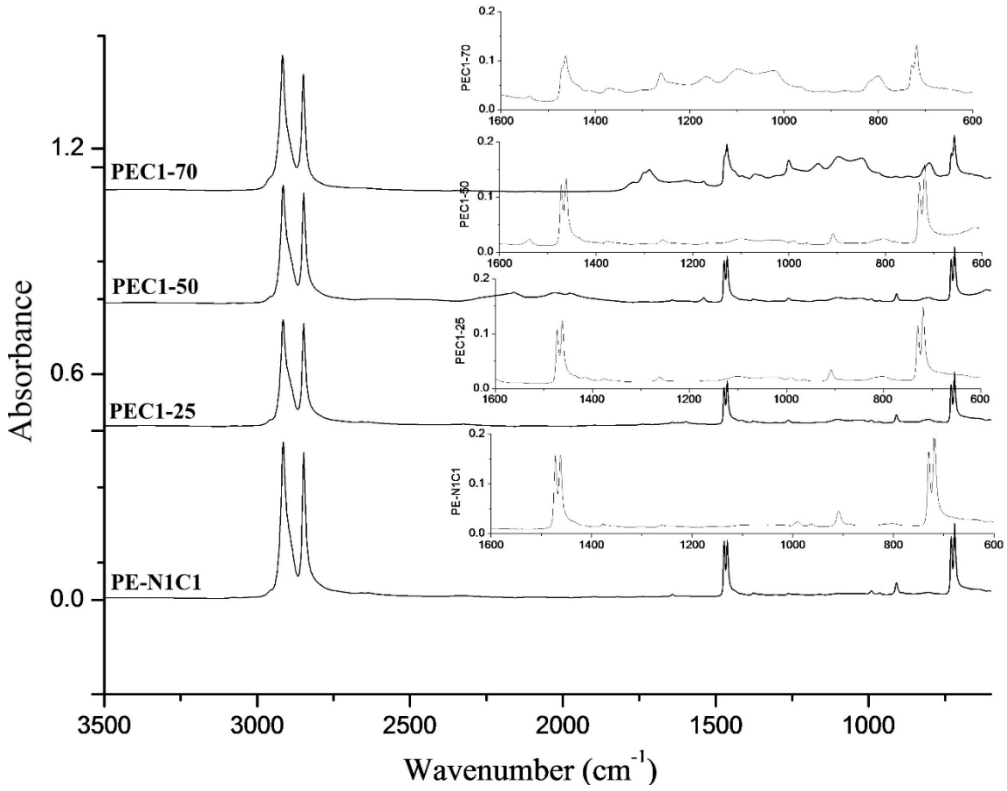

Figure 9 The FTIR spectra of the resulting PE using **N1C1** and **C1**.

From the ^{13}C NMR spectra, the integrated peaks of polyethylenes [40] showed that **N1C1** and **C1** enchained methyl, ethyl, propyl, and butyl branches/1,000 C atoms in different concentrations. A high percentage of short-chain branches suggested the contribution of Ni catalytic centers according to the different conditions of polymerization.

In many cases, obtaining the desired multimodal polymers by mixing individual mononuclear catalysts was not possible. The heterotrinuclear catalyst {Ti_2Ni} evaluated here might be a useful catalyst precursor for synthesizing such materials, as it can copolymerize ethylene with higher α-olefins produced *in situ*. Therefore, the Ni species preferably produced α-olefins with shorter chains at room temperature, where the percentage of higher oligomers in the reaction solution was low. The insertion of short chains of α-olefins was favored by the synergic effect between Ti···Ni sites, resulting in copolymerization through only one monomer.

Scheme 1 shows a predicted propagation mechanism, β-H elimination, and branching produced at the Ni sites. Depending on the temperature, the termination of chain growth occurs via β-H elimination, chain transfer to the monomer, or chain transfer to the cocatalyst. Additionally,

branching might occur due to the reinsertion of vinyl end-groups (macromonomers) by the chain walking mechanism, allowing the growing center to migrate along the polymer chain [41]. If β-H elimination is the dominant chain-transfer pathway, chain transfer to monomers or cocatalysts is negligible [42].

According to Scheme 1, branching increases due to the recapture of the vinyl-end groups of the polymer at the neighboring Ti sites after chain transfer from the Ni sites. This process facilitates intramolecular reinsertion into the growing polymer chain. Moreover, it implies bimodal polydispersity.

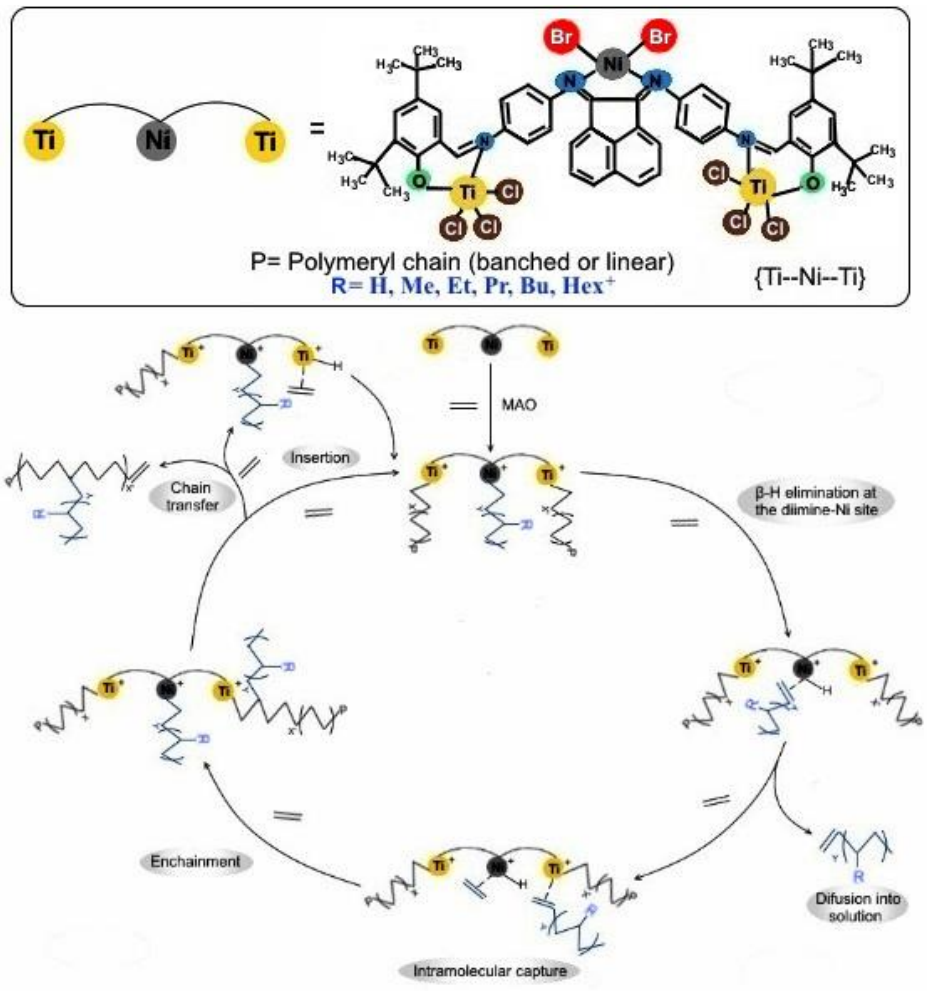

Scheme 1 The steps proposed for the heterotrinuclear cooperation between Ti···Ni sites to produce polyethylenes with the insertion of comonomers *in situ.*

4. Conclusions

The properties related to the synthesis, characterization, and polymerization of the mononuclear **N1C1** and heterotrinuclear **C1** precatalysts were investigated. A heterotrinuclear catalyst was synthesized using early and late transition metals to enhance the catalytic efficiency. The properties of the polymers imparted by different metal centers were incorporated into the same polymer product. The structures were studied by DFT calculations at the B3LYP/LACVP** level. According to our calculations, the titanium(IV) centers were in a slightly distorted trigonal bipyramidal environment, and the average Ti···Ni distance was 8.76 Å.

This catalyst produced methyl, ethyl, propyl, and butyl branched polyethylenes in different proportions according to the applied temperature from an ethylene monomer, which was used as the only feedstock. The heterotrinuclear **C1** precatalyst had a higher molecular weight and used a lower concentration of MAO than the mononuclear **N1C1** precatalyst. However, it had lower activity, probably due to steric and electronic effects. The development of a new catalyst implied opportunities to synthesize novel catalysts and polymers with unique microstructures. These might have new applications because of the ability of the Ti sites to copolymerize short-chain α-olefins produced by the Ni sites through *in situ* copolymerizations, which might be used for producing copolymers using ethylene as the only monomer.

Acknowledgments

The authors thank the Brazilian Council for Scientific and Technological Development (CNPq), the Coordination for the Improvement of Higher Education Personnel (CAPES), and the Carlos Chagas Filho Foundation for Supporting Research in the State of Rio de Janeiro (FAPERJ) for the financial support.

Author Contributions

Luiz Felipe da M. Rocha: Conceptualization, Methodology, Validation, Investigation, Writing - Original Draft, Visualization. Leonardo C. Ferreira: Conceptualization, Methodology, Validation, Investigation, Writing - Review & Editing, Visualization. Maria de Fátima Vieira Marques: Conceptualization, Methodology, Resources, Writing - Review & Editing, Supervision. Rodrigo S. Bitzer: Conceptualization, Validation, Writing - Review & Editing, Visualization. Marco Antonio Chaer Nascimento: Conceptualization, Validation, Writing - Review & Editing, Visualization.

Funding

CNPq, Capes and Faperj.

Competing Interests

The authors have declared that no competing interests exist.

Additional Materials

The following additional materials are uploaded at the page of this paper.

1. Figure S1: UV-Vis absorbance spectrum of the N1C2 complex.
2. Figure S2: UV-Vis absorbance spectrum of the C1 complex.
3. Figure S3: ^{13}C-NMR spectrum of PE-N1C1.
4. Figure S4: ^{13}C-NMR spectrum of PE-C125.
5. Figure S5: ^{13}C-NMR spectrum of PE-C150.
6. Figure S6: ^{13}C-NMR spectrum of PE-C170.

References

1. Haak RM, Wezenberg SJ, Kleij AW. Cooperative multimetallic catalysis using metallosalens. Chem Commun (Camb). 2010; 46: 2713-2723.
2. Maity R, Birenheide BS, Breher F, Sarkar B. Cooperative effects in multimetallic complexes applied in catalysis. ChemCatChem. 2021; 13: 2337-2370.
3. McInnis JP, Delferro M, Marks TJ. Multinuclear group 4 catalysis: Olefin polymerization pathways modified by strong metal-metal cooperative effects. Acc Chem Res. 2014; 47: 2545-2557.
4. Zaera F. Designing sites in heterogeneous catalysis: Are we reaching selectivities competitive with those of homogeneous catalysts? Chem Rev. 2022; 122: 8594-8757.
5. Qu R, Suo H, Gu Y, Weng Y, Qin Y. Sidechain metallopolymers with precisely controlled structures: Synthesis and application in catalysis. Polymers (Basel). 2022; 14: 1128.
6. Gao Y, Mouat AR, Motta A, Macchioni A, Zuccaccia C, Delferro M, et al. Pyridylamido bi-hafnium olefin polymerization catalysis: Conformationally supported Hf⋯ Hf enchainment cooperativity. ACS Catal. 2015; 5: 5272-5282.
7. Khoshsefat M, Ma Y, Sun WH. Multinuclear late transition metal catalysts for olefin polymerization. Coord Chem Rev. 2021; 434: 213788.
8. Durand DJ, Fey N. Building a toolbox for the analysis and prediction of ligand and catalyst effects in organometallic catalysis. Acc Chem Res. 2021; 54: 837-848.
9. Li H, Li L, Marks TJ, Liable-Sands L, Rheingold AL. Catalyst/cocatalyst nuclearity effects in single-site olefin polymerization. Significantly enhanced 1-octene and isobutene comonomer enchainment in ethylene polymerizations mediated by binuclear catalysts and cocatalysts. J Am Chem Soc. 2003; 125: 10788-10789.
10. Doyle DJ, Gibson VC, White AJP. Synthesis and structures of bimetallic and polymeric zinc coordination compounds supported by salicylaldiminato and anilido-aldimine ligands. Dalton Trans. 2007; 21: 358-363.
11. Liu S, Motta A, Mouat AR, Delferro M, Marks TJ. Very large cooperative effects in heterobimetallic titanium-chromium catalysts for ethylene polymerization/copolymerization. J Am Chem Soc. 2014; 136: 10460-10469.
12. Suo H, Solan GA, Ma Y, Sun WH. Developments in compartmentalized bimetallic transition metal ethylene polymerization catalysts. Coord Chem Rev. 2018; 372: 101-116.
13. Xiao A, Pan L, Shibao Z, FeiFei W. Symmetric and asymmetric binuclear α-diimine nickel(II) complexes for ethylene polymerization. Iran J Chem Chem Eng. 2019; 38: 137-144.
14. Kaminsky W. New polymers by metallocene catalysis. Macromol Chem Phys. 1996; 197: 3907-3945.
15. Kim SH, Tewell CR, Somorjai GA. Surface science studies of Ziegler-Natta olefin polymerization system: Correlations between polymerization kinetics, polymer structures, and active site structures on model catalysts. Korean J Chem Eng. 2002; 19: 1-10.
16. Johnson LK, Killian CM, Brookhart M. New Pd(II)- and Ni(II)-based catalysts for polymerization of ethylene and .alpha.-olefins. J Am Chem Soc. 1995; 117: 6414-6415.
17. Killian CM, Johnson LK, Brookhart M. Preparation of linear α-olefins using cationic nickel(II) α-diimine catalysts. Organometallics. 1997; 16: 2005-2007.

18. Svejda SA, Brookhart M. Ethylene oligomerization and propylene dimerization using cationic (α-diimine)nickel(II) catalysts. Organometallics. 1999; 18: 65-74.
19. Matsui S, Mitani M, Saito J, Tohi Y, Makio H, Matsukawa N, et al. A family of zirconium complexes having two phenoxy-imine chelate ligands for olefin polymerization. J Am Chem Soc. 2001; 123: 6847-6856.
20. Matsui S, Mitani M, Saito J, Tohi Y, Makio H, Tanaka H, et al. Post-metallocenes: A new bis(salicylaldiminato) zirconium complex for ethylene polymerization. Chem Lett. 1999; 28: 1263-1264.
21. Makio H, Fujita T. Synthesis of chain-end functionalized polyolefins with a bis(phenoxy imine) titanium catalyst. Macromol Rapid Commun. 2007; 28: 698-703.
22. Yuan SF, Yan Y, Solan GA, Ma Y, Sun WH. Recent advancements in N-ligated group 4 molecular catalysts for the (co)polymerization of ethylene. Coord Chem Rev. 2020; 411: 213254.
23. Wang Z, Liu Q, Solan GA, Sun WH. Recent advances in Ni-mediated ethylene chain growth: Ni_{mine}-donor ligand effects on catalytic activity, thermal stability and oligo-/polymer structure. Coord Chem Rev. 2017; 350: 68-83.
24. Nifant'ev IE, Ivchenko PV, Vinogradov AA. Heterocycle-fused cyclopentadienyl metal complexes: Heterocene synthesis, structure and catalytic applications. Coord Chem Rev. 2021; 426: 213515.
25. Ferreira LC, Filgueiras CAL, Visentin LC, Bordinhão J, Hörner M. One-pot preparation, spectroscopic and structural characterization of mercury(II) complexes of bulky diimines with halides and pseudohalides. Z Anorg Allg Chem. 2008; 634: 1896-1900.
26. JAGUAR Version 7.9. New York: Schrödinger; 2011.
27. Becke AD. Density-functional thermochemistry. III. The role of exact exchange. J Chem Phys. 1993; 98: 5648-5652.
28. Harlin A, Vainio T. Effect of polydispersity on the thermo-mechanical degradation of HDPE polymerized using a chromium catalyst. Polym Degrad Stab. 1993; 39: 29-34.
29. Rocha LF, Ferreira LC, Marques MF. Synthesis and evaluation of arylimino pyridine nickel(II) catalysts: Influence of substituents on polyethylene structure. Chem Chem Technol. 2015; 9: 421-428.
30. Visentin LC, Ferreira LC, Bordinhão J, Filgueiras CAL. Synthesis, structural and spectroscopic studies of novel azo-containing N,O-bonded complexes in the α-iminoketone and azophenolate forms. J Braz Chem Soc. 2010; 21: 1187-1194.
31. Nakamoto K. Infrared and Raman spectra of inorganic and coordination compounds: Part A: Theory and applications in inorganic chemistry. 6th ed. New York: John Wiley & Sons; 2009.
32. Orpen AG, Brammer L, Allen FH, Kennard O, Watson DG, Taylor R. Supplement. Tables of bond lengths determined by X-ray and neutron diffraction. Part 2. Organometallic compounds and co-ordination complexes of the d- and f-block metals. J Chem Soc Dalton Trans. 1989: S1-S83. doi: 10.1039/DT98900000S1.
33. Addison AW, Rao TN, Reedijk J, van Rijn J, Verschoor GC. Synthesis, structure, and spectroscopic properties of copper(II) compounds containing nitrogen-sulphur donor ligands; the crystal and molecular structure of aqua[1,7-bis(N-methylbenzimidazol-2'-yl)-2,6-dithiaheptane]copper(II) perchlorate. J Chem Soc Dalton Trans. 1984: 1349-1356. doi: 10.1039/DT9840001349.
34. Hoffman AJ, Mills G, Yee H, Hoffmann MR. Q-sized cadmium sulfide: Synthesis, characterization, and efficiency of photoinitiation of polymerization of several vinylic monomers. J Phys Chem. 1992; 96: 5546-5552.

35. Buchwalter P, Rosé J, Braunstein P. Multimetallic catalysis based on heterometallic complexes and clusters. Chem Rev. 2015; 115: 28-126.
36. Brookhart MS, Johnson LK, Killian CM, McCord EF, McLain SJ, Kreutzer KA, et al. Olefin polymers. Wilmington: EI Du Pont de Nemours and Company; 1999; US5880241A.
37. Brookhart MS, Johnson LK, Killian CM, Arthur SD, Feldman J, McCord EF, et al. Processes of polymerizing olefins. EI Du Pont de Nemours and Company, University of North Carolina; 1999; US5866663A.
38. Striegel AM. Multiple detection in size-exclusion chromatography. Washington, DC: ACS; 2004.
39. Gulmine JV, Janissek PR, Heise HM, Akcelrud L. Degradation profile of polyethylene after artificial accelerated weathering. Polym Degrad Stab. 2003; 79: 385-397.
40. Liu W, Ray III DG, Rinaldi PL. Resolution of signals from long-chain branching in polyethylene by ^{13}C NMR at 188.6 MHz. Macromolecules. 1999; 32: 3817-3819.
41. Jurkiewicz A, Eilerts NW, Hsieh ET. ^{13}C NMR characterization of short chain branches of nickel catalyzed polyethylene. Macromolecules. 1999; 32: 5471-5476.
42. Liu Z, Somsook E, White CB, Rosaaen KA, Landis CRJ. Kinetics of initiation, propagation, and termination for the [rac-(C_2H_4(1-indenyl)$_2$)ZrMe][MeB(C_6F_5)$_3$]-catalyzed polymerization of 1-hexene. J Am Chem Soc. 2001; 123: 11193-11207.